La mer 34: 45–55, 1996
Société franco-japonaise d'océanographie, Tokyo

Examples of ocean wave spectra estimated from ERS-1 SAR images

Li-Guang LEU*,*** Yi-Yu KUO** and Cho-Teng LIU***

Abstract: ERS-1 SAR (Synthetic Aperture Radar) images were used to derive ocean wave spectra. Because of the simplicity in bottom topography and availability of sea truth data, Hwalien coastal region east of Taiwan was selected as the site for comparing the satellite SAR-derived and the *in situ* surface wave spectra. Two-dimensional (2D) wavenumber spectra were derived from the digital SAR images through the Fourier transformation in the space domain. The wavelengths, wavenumber, wave period and the direction of dominant wave systems were then calculated from the spectral peaks. To verify these SAR-derived wave characteristics, the wavenumber spectra were converted to the frequency power spectra for direct comparison with simultaneously observed *in situ* wave spectra. Two cases were studied. The difference between the SAR-derived wave directions and those measured by the directional wave rider buoy was about 8° and 26°, and about 3.5% and 16% for the wavelength. Since the significant wave height measured by the wave-rider was only 0.73 m and 1.65 m, we can conclude that using satellite SAR to observe the ocean waves is a feasible approach with acceptable accuracy, even over a relatively calm sea.

1. Introduction

Observing ocean surface waves using conventional instruments, e.g., the wave gauges, wave-riders, and ultrasonic wave meter, is relatively difficult at sea. Such difficulty includes deploying, monitoring and retrieving these instruments, thereby hindering efforts to acquire continuous wave data. The amount of surface wave data is much less than expected owing to the loss, damage, and malfunction of the instruments. Besides, most conventional wave instruments record the temporal change of sea surface elevation to derive the surface wave spectra, only a few can observe the spatial characteristics of wave fields. In contrast, the remote sensing technique can obtain the information of ocean wave-field at synoptic scale, subsequently making it complementary to the conventional methods.

Synthetic Aperture Radar (SAR) images have been used to observe ocean surface waves (GONZALES *et al.*, 1979) since launching of the satellite SEASAT in 1978. The visible bands of System Probatoire d'Observation de la Terre (SPOT) can be used to image ocean surface wave-field (POPULUS, 1991); however, it functions only in the daytime and on a cloud-free day. SAR is an active radar. The microwave pulses sent out by the radar can penetrate the cloud and moisture in the air, and interact with the ocean surface waves – regardless of the time of the day or the weather conditions. Hence, SAR images can be used for monitoring the wave-field of rough seas, especially near regions where typhoons frequently occur. This capability is quite useful for the safe and economic design of coastal marine structures. Despite some successful applications of SAR images in previous case studies on bottom topography, eddy, internal wave, current and boundary, ship wakes, a definitive algorithm h as not yet been derived for imaging ocean surface waves by SAR. The SAR image spectrum

* Energy & Resources Laboratories, Industrial Technology Research Institute, Bldg. 24, 195-6, Chung-Hsing Rd. Sec. 4, Hsinchu, Taiwan 310, Republic of China
** Institute of Civil Engineering, National Chiao-Tung University, Hsinchu, Taiwan, Republic of China
*** Institute of Oceanography, National Taiwan University, Taipei, Taiwan, Republic of China.

is actually not representative of the spectrum of sea surface displacement. The power spectra of SAR image is only a transformation of a directional slope spectrum of sea surface through a modulation transfer function (MTF) (ALPERS and HASSELMANN, 1978). The SAR imaging of the sea surface is conceivably affected by the surface wave motion ; however, its mechanism is not yet fully understood (ALPERS *et al.*, 1981 ; HASSELMANN, 1985 ; ALPERS and BRÜNING, 1986). Many studies on how surface wave motions affect SAR imging mechanism are still underway.

Earlier studies of the wave-field with satellite sensors were under taken primarily on the open seas. Relatively few successful ovservations were made of ocean surface waves near shore by satellite SAR. The images of apparent wavelike pattern were not easily obtained at low sea conditions in which the significant wave height was below 2 meters (GONZALES, 1979). The simple dispersion relation for deep water waves used in transferring the wave-number power spectra to the frequency power spectra. However, the general dispersion relation must be used in a coastal region.

In this study, two SAR images over the eastern coast of Taiwan are analyzed and compared with *in situ* wave data recorded simultaneously by a wave-rider. the wave-rider was located about 1 km offshore from the Hwalien Harbor on the east coast of Taiwan (Fig. 1). The water depth is about 26 m at the site of wave-rider. The waves are considered as intermediate water waves because the wavelength of swell east of Taiwan is normally around about one hundred meters. The significant wave heights were beloe 2 meters at the time of SAR observation. Subscenes of the SAR images (Fig. 2) covering the site of the wave-rider are extracted for the study. Also, preprocessing techniques such as detrend and low pass filtering are used to improve the signal to noise ratio (SNR) and to enhance the spectral characteristics. Figure 3 provides the data processing flow chart and also compares both spectra derived from SAR images and *in situ* wave data.

2. Data and pre-processing

2.1. ERS-1 SAR data and in situ data

The European Space Administration (ESA) launched the first European Remote Sensing Satellite (ERS-1) in July 1991, with the primary mission of ocean survey and research. The SAR scans and receives radar echoes from the sea surface at an angle of 23° off-nadir with an altitude of 785 km. The microwave used by SAR is C-band at 5.3 GHz. Every full scene of SAR images spans an area of around 100 km×100 km. All pixels are nearly square with a size of 12.5m by 12.5m. The ERS-1 SAR images used in this study were received by the Ground Station at the Center for Space and Remote Sensing Research (CSRSR), National Central University in Chungli, Taiwan. Obtaining the image for averaging four looks is the major objective. The geometrically uncorrected four-look images are generally referred to as georeference or slant range data. SAR images have two mo des : discending and ascending. In the descending mode, the satellite passes over Taiwan at about 2 : 30 Universal Time Coordinated (UTC), or 10 : 30 Taiwan Local Time (TLT). The original SAR images are reversed in the east-west direction, similar to a mirror image of the map. In the ascending mode, ERS-1 passes over Taiwan at about 14 : 30 UTC, or 22 : 30 TLT. Before re-mapping, the SAR images are turned upside down from a regular map view. In this study, two images were acquired from CSRSR. The acquisition time of SAR images and their orbit numbers are (a) descending orbit 12358, track 189 on November 26, 1993, 2 : 25 UTC, or 10 : 25 TLT, and (b) ascending orbit 122, track 31 on November 15, 1993, 14 : 19 UTC, or 22 : 19 TLT.

The Institute of Harbor and Marine Technology (IHMT) of Taiwan collected the *in situ* wave data. A wave-rider buoy was deployed at (24°0′00″N, 121°38′24.5″E), outside of the east breakwater of Hwalien Harbor. The sampling rate of the wave-rider was 1.28 Hz and the sea surface elevation was recorded for twenty minutes at two hour intervals. The data were then transmitted in at VHF frequency to the receiver in a building near the coast. Next, wave data were translated and transferred to a personal computer for recording. Acceleration of

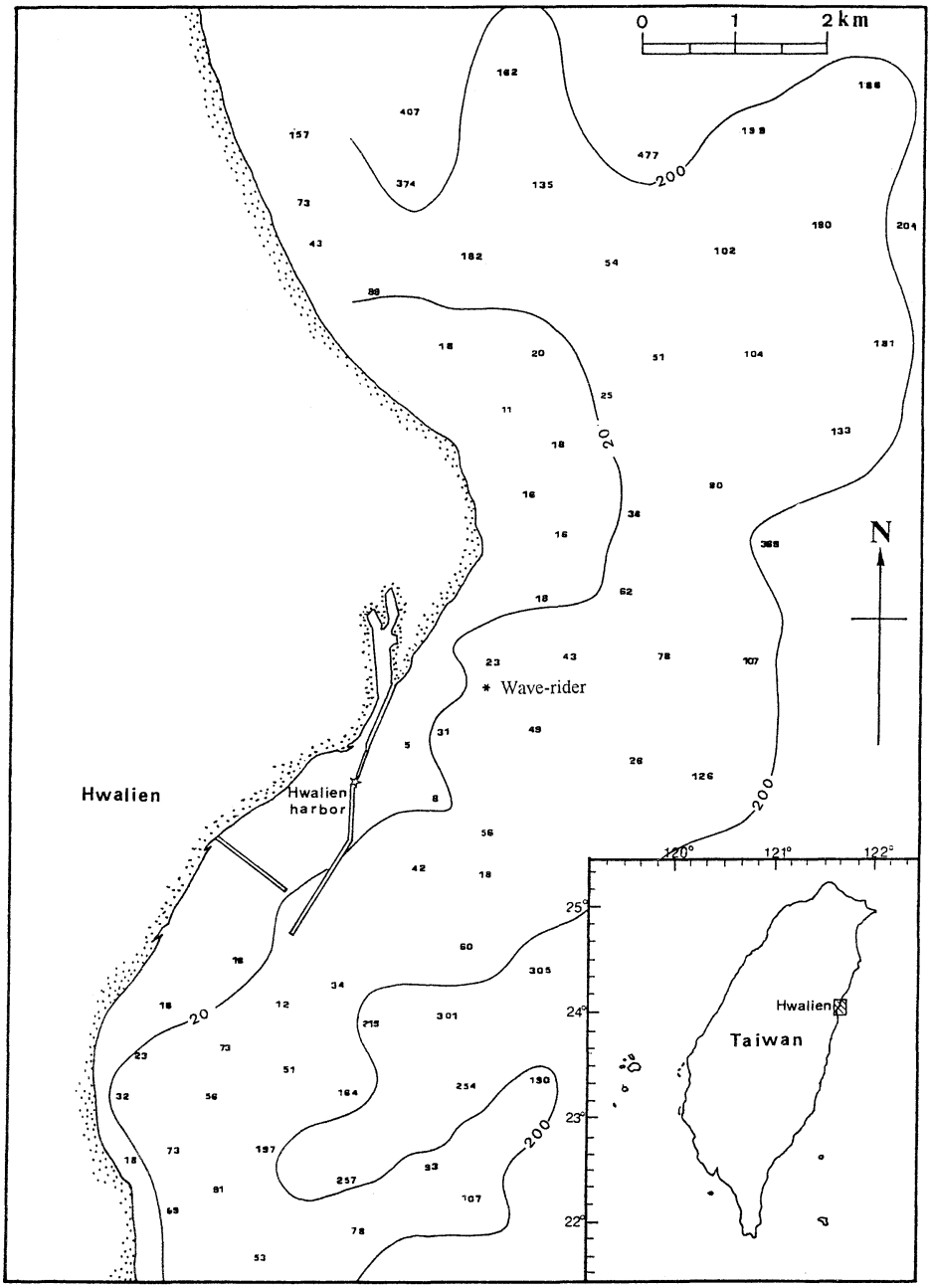

Fig. 1. The location of wave-rider and the bathymetry near Hwalien. Depths are in meters.

the buoy was measured by two fixed accelerometers in the horizontal x and y directions, and by an accelerometer mounted on a gravity stabilized platform in the vertical z direction. Also, the sea surface elevation was derived from the heave motion of the buoy. Moreover, the wave direction was derived from the horizontal acceleration of the buoy. Two sets of *in situ* wave data were collected on (a) November 26, 1993, 10 : 30 TLT, and (b) No vember 15, 1993, 22 : 24 TLT.

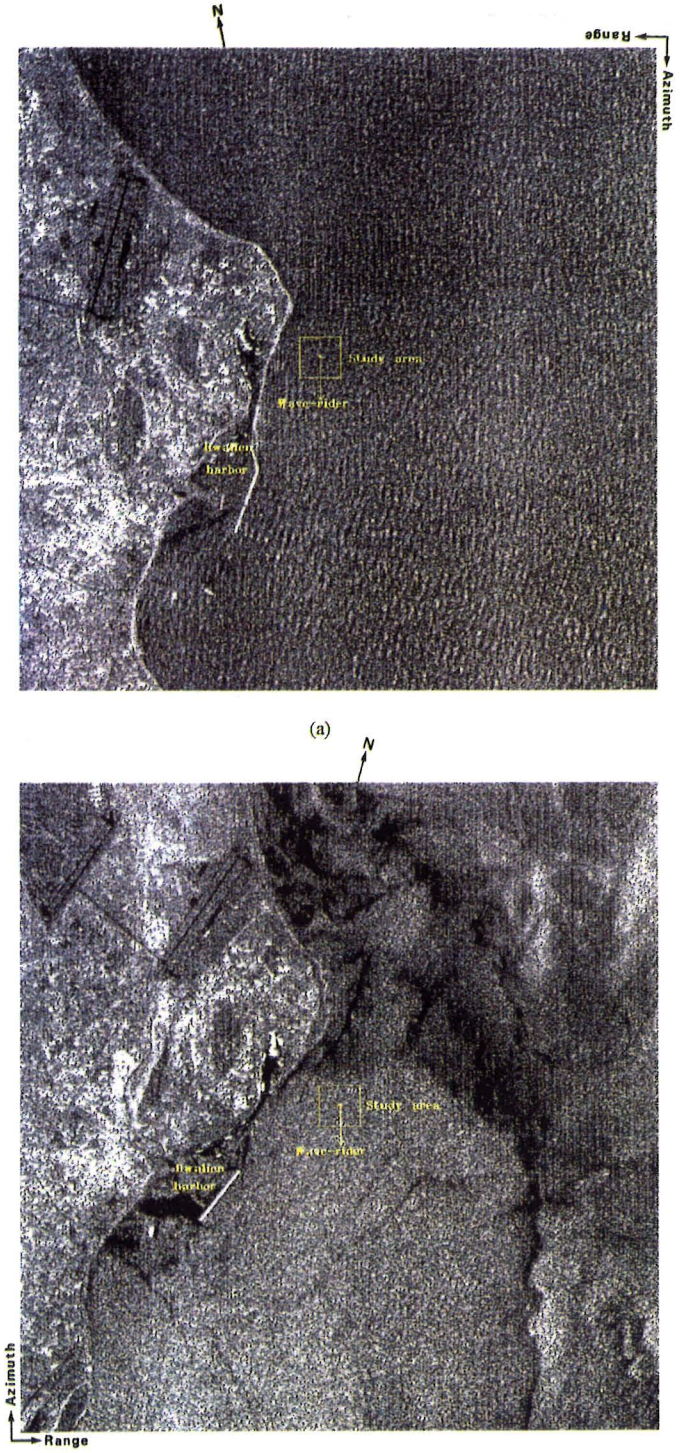

Fig. 2. ERS-1 SAR images over Hwalien of Taiwan for case (a) descending orbit 12358 on November 26, 1993, and case (b) ascending orbit 122 on November 15, 1993

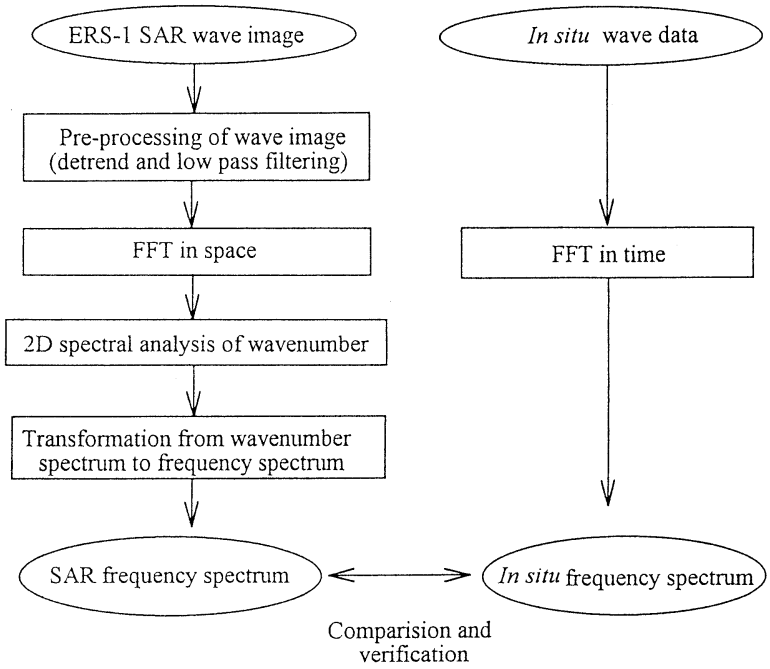

Fig. 3. Flow chart of data processing and their comparison of spectra derived from ERS-1 SAR images and *in situ* wave data.

2.2. SAR wave image pre-processing

Some appropriate filterings are necessary before the wave spectral analysis of the satellite images can be performed. A low pass filter was used to remove the high frequency noises that are typical in SAR images : a high pass filter was applied to remove the trend of grayness in the satellite images. The echo strength recorded by the SAR varies from pixel to pixel, as in the case of the distance between the satellite and the sea surface. The noises in the satellite images are regarded as a random error. A moving average with a 3 by 3 mask is sufficient to reduce the random error. The removal of noise improves the SNR of the satellite-derived surface wave systems. The nearshore wave-field is normally inhomogeneous owing to the topographic steering of the swell. Taking a small subscene of the wave image is preferable in the sense that the wave-field is nearly homogeneous in the subscene, thereby yielding stable statistics and power spectra of the wave system. The detrend of wave images may make SAR images of a wavelike pattern more easily observed and manifest a small variation of signals thereby, producing an enhanced wave power spectra.

The digital counts of SAR images represent the radar backscattering crosssection of the sea surface. Assume that the gradual change of gray tone in an image can be expressed as

$$X_t(m_1, m_2) = a + bm_1 + cm_2 \quad (1)$$

where a, b, c are constants, and m_1 m_2 fall within 0 to N-1, and (m_1, m_2) is the position in the image of N by N pixels. The spatial 2D linear least square method is used to obtain the trend of wave image. The detrended image is obtained after removing the main trend image. If the matrix of original digital image is expressed as $X_0(m_1, m_2)$, the matrix of detrended image is written as

$$X(m_1, m_2) = X_0(m_1, m_2) - X_t(m_1, m_2) \quad (2)$$

The process of detrending may not be enhanced for every wave-field image. Detrending may occasionally more effective in obtaining the actual wave pattern in images with an unever backscattering cross-section. However, manipulating the later processing of the SAR

images after detending and deriving the enhanced wavenumber power spectra are highly desired.

3. Methodology

3.1. Spatial fourier transform

A SAR image is a 2D sampling of the backscattering strength of satellite radar echoes of the sea surface over an area of 100 km by 100 km. The subscene covers the wave-rider location with a relatively uniform wave pattern so that a reliable conclusion can be derived from the comparison between the SAR data with *in situ* wave data. All of the pixels are assumed here to be squares of length d on each side. As shown in equation (2), let $X(m_1m_2)$ be the digital value of a pixel located at (m_1m_2) within the subscene of N by N pixels. Here, the 2D Discrete Fourier Transform (DFT) is used to derive the wavenumber spectra from the SAR images. DFT defines

$$E(n_x \cdot k_0 \cdot n_y \cdot k_0) = \frac{1}{N^2} \sum_{m_2=0}^{n-1} \left[\sum_{m_1=1}^{n=1} X(m_1, m_2) \cdot e^{-in_x k_0 \cdot m_1 \cdot \Delta x} \right] \cdot e^{-in_y \cdot k_0 \cdot m_1 \cdot \Delta\Delta x} \quad (3)$$

where

$k_0 = 2\pi / D$

$D = N \cdot d$ = the linear size of the subscene of the SAR image

d = 12.5 meters

N = 64 in following studies

$n_x \cdot k_0 = k_x$ = wavenumber in x direction

$n_y \cdot k_0 = k_y$ = wavenumber in y direction

n_x and n_y = 1, 2, 3, ……N

Computations were performed via Fast Fourier Transforms (FFT), thereby, subsequently limiting the choice of N to the power of 2, i.e. $N = 2^p (p = 1, 2, \cdots)$. The power spectra were acquired in correspondence to the wavenumbers in the x and y directions, respectively. The units for the wavenumber coordinates are

$$\delta k_x = \delta k_y = 2\pi / D = 2\pi / (N \cdot d).$$

3.2. Wavenumber spectrum

In the 2D wavenumber spectrum, the spectral peak (n_x, n_y) represents the dominant wave characteristics, i.e.,

$$\frac{2\pi}{L} = K = \sqrt{K_x^2 + K_y^2} \quad (4)$$

$$\tan\theta = \frac{K_y}{K_x} = \frac{n_y}{n_y} \quad (5)$$

where K is the wavenumber of dominant wave. K_x and K_y are their components in x and y directions so that

$$L = \frac{D}{\sqrt{n_x^2 + n_y^2}} = \text{the wavelenght of dominant wave} \quad (6)$$

$$\theta = \tan^{-1}\left(\frac{n_y}{n_x}\right) = \text{the wave direction of dominant wave counterclockwise from } k_x \quad (7)$$

A one-dimensional wavenumber power spectrum can be derived by integrating the 2D wavenumber power spectrum in all directions. The spectral peak of a one-directional wavenumber power spectrum shows the wavelenght of the dominant wave system. The variations of wave slopes shown in the SAR digital image were not the absolute wave heights. On the other hand, wave height can be calculated from *in situ* data via zero-up crossing method or spectral analysis. Following carefu. calibration of the wavenumber spectra with many simultaneously collected SAR and *in situ* data, the wave height may be calculated from the spectra of SAR images. The wave height can still not be accurately dirived from SAR data since the effects of wave motion mechanism in SAR images remain unclear.

3.3. Frequency power spectrum

Time-series data analysis is the conventional approach of observing ocean waves with wave-rider buoys. The wavenumber power spectra are derived from SAR images of spatial data, thereby making a direct comparison with the frequency power spectra derived from *in situ* wave data nearly impossible. The wavenumber power spectra should be transformed to frequency power spectra, while the reverse can not be done because of the difference in the number of independent variables. The wavenumber power spectra in the Cartesian coordinate system and in the polar coordinate system have the following relationship (TUCKER, 1991) :

$$\phi(k,\theta)=k\cdot\phi(k_x,k_y) \tag{8}$$

where Ψ is the wavenumber power spectrum derived from SAR images, k is the wavenumber of ocean surface waves in SAR images and $k=\sqrt{k_x^2+k_y^2}$

The total wave energy computed from the frequency(f) domain and the wavenumber(k) domain should be equal, i.e.,

$$\int_0^{\infty}\int_0^{2\pi}\phi(f,\theta)\cdot df\cdot d\theta=\int_0^{\infty}\int_0^{2\pi}\phi(k,\theta)\cdot dk\cdot d\theta \tag{9}$$

where $\phi(f,\theta)$ is SAR directional frequency power spectrum, and is determined in the following derivation

Therefore,

$$\phi(f,\theta)=\phi(k,\theta)\cdot\frac{dk}{df} \tag{10}$$

By combining (8) and (10), the relationship between directional frequency power spectrum and wavenumber power spectrum is

$$\phi(f,\theta)=\phi(k_x,k_y)\cdot k\cdot\frac{dk}{df} \tag{11}$$

$\frac{dk}{df}$ in equation (11) can be calculated via the wave dispersion relation :

$$\omega^2=(2\pi f)^2=gk\tan h\,(kh) \tag{12}$$

where ω is the angular frequency of wave
g is the acceleration of gravity
h is the water depth of the study area

By considering the case of uniform water depth h, the omnidirectional frequency power spectrum $\Phi(f)$ can be calculated by integrating the directional frequency power spectrum over all directions :

$$\Phi(f)=1/(2\pi)\int_0^{2\pi}\phi(f,\theta)\cdot d\theta \tag{13}$$

The forms and peaks in frequency power spectra of SAR images and *in situ* wave data are compared in the following to assess the feasibility of using SAR images to estimate the characteristics of ocean wave-field over coastal zone.

4. Case studies

The SAR images of Hwalien over the east coastal region of Taiwan were chosen to analyze the wave-field characteristics. A wave observation station was located at the offshore of Hwalien harbor. Comparing the SAR images with *in situ* wave data simultaneously collected in the same study area was relatively easy. CSRSR provided the ERS-1 SAR images over Hwalien. Two ERS-1 SAR images were acquired during the phase C (35 day repeat cycle) of ERS-1 operation.

SAR images of Figs. 2a and 2b show the different sea states of case (a) and (b). The sea states near Hwalien are largely affected by the north-east monsoon during the autumn and winter seasons. The wave height is usually about 1 m to 2 m and, in 1993, was larger than 2 m at only about 30% of the time. The wave period is generally 6 sec to 8 sec. The worst sea states appear from August to October when the typhoons approach from the east. Figure 1 shows the location of Hwalien in Taiwan and the nearshore bottom topography. The water depth changes rapidly offshore. The wave-field in the coastal zone is relatively localized. The wave spectra observed by the wave-rider may not be representative for a large SAR image. On the other hand, the wavenumber power spectra lose their statistic characteristics if the subscene is too small to contain a sufficient number of waves. A subscene of 64 pixels by 64 pixels (or 800 m by 800 m) is considered optimal, based on our previous experimental studies. Twodimensional wavenumber power spectra were derived via FFT of the SAR data in the space domain. Figure 4 shows the wavenumber power spectra of case (a) and (b). Results obtained from the case studies and the comparison between SAR data and *in situ* wave data are discussed below.

4.1. Case(a) : wave field on November 26, 1993

The 2D wavenumber power spectrum in Fig. 4a was derived from the Fourier transform of a 800 m by 800 m subscene of the satellite image in Fig. 2a. The spectral peak located at $(n_x, n_y)=(2,5)$ represents the primary wave system east of Taiwan on November 26, 1993. The direction of k_x axis is 12.9° in a clockwise direction from the south for all descending pass of ERS-1, as in case (a). The wave came from a 68° counter-clockwise direction of k_x or 125° from the north. The wavenumber of the primary wave system is 4.23×10^{-2} rad/m, corre-

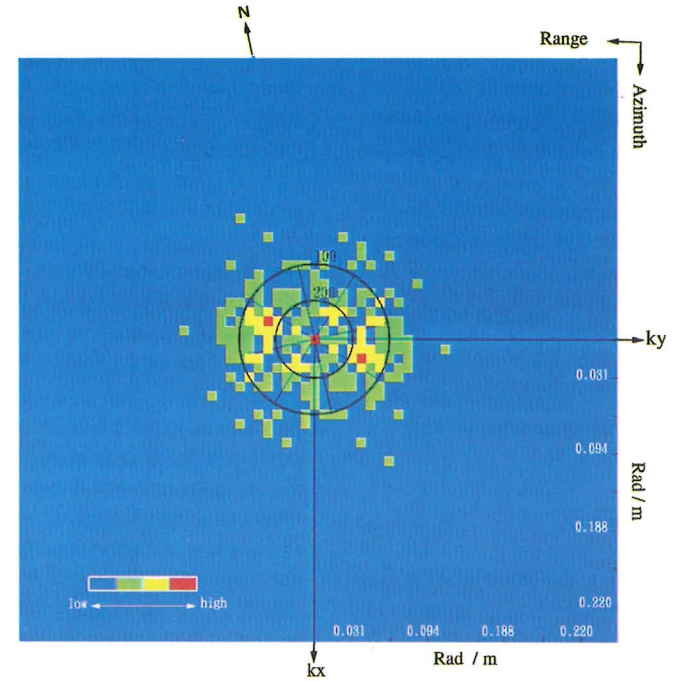

(a)

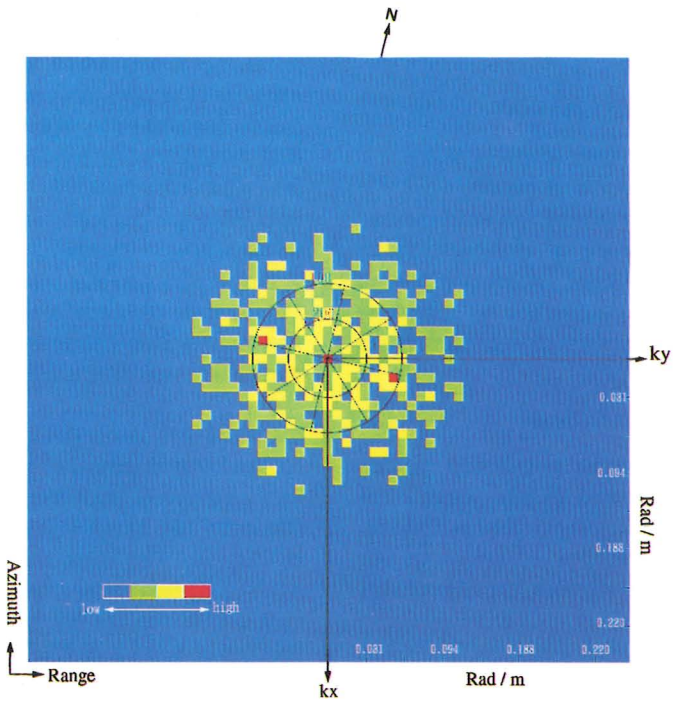

(b)

Fig. 4. SAR wavenumber power spectra of Hwalien coastal zone for case (a) and (b). The inner and outer circles denote the loci of wavelength 200 m and 100 m, respectively.

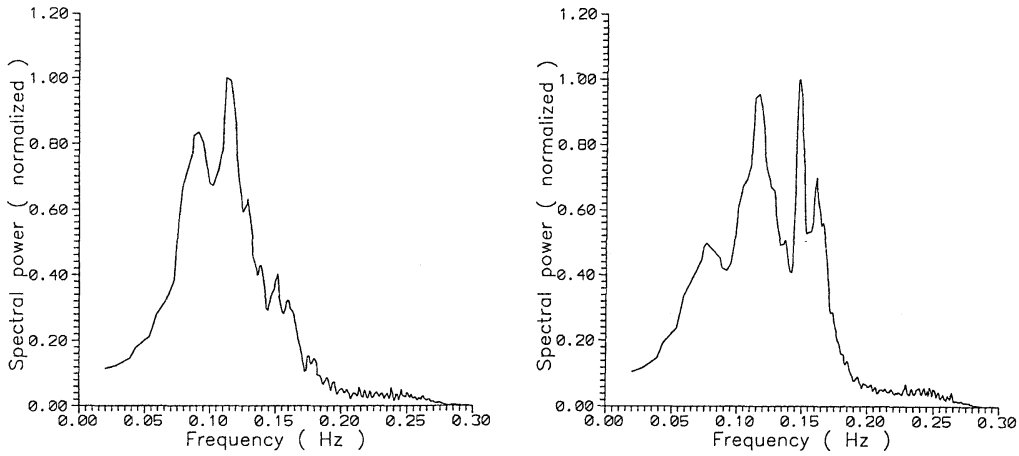

Fig. 5. SAR frequency power spectra of Hwalien coastal zone for case (a) and (b).

sponding to 149 m in wavelength. This 2D wavenumber power spectrum was transformed to the omnidirectional frequency power spectrum by integrating the power spectra of equal-wavelength waves in all directions. Figure 5a clearly reveals two separate peaks (fp) in the frequency power spectrum : one is at 0.092 Hz and the other is at 0.113 Hz. The wave system with fp=0.092 Hz in the omnidirectional frequency power spectrum matches the wave system of $(n_x, n_y)=(2, 5)$ in the 2D wavenumber spectrum. The other one with fp=0.113Hz (wavelength=110m) does not distinguish itself in the 2D wavenumber power spectrum. Further analysis reveals a large but narrow spectral peak appearing at the wavenumber $(n_x, n_y)=(-2, 7)$ in Fig. 4a. This wave system came from 106° in a counterclockwise direction from the k_x axis, or 87° in a clockwise direction from the north.

To verify the SAR-derived wave system, *in situ* wave data acquired by the wave-rider were analyzed. Figure 6a shows two peaks of frequency power spectrum : one with a frequency of 0.095 Hz and the other with a frequency of 0.11 Hz. Those peaks correspond to wave periods of 10.53 sec and 9.09 sec, and wavelengths of 141m and 114m, respectively. The solid line in Fig. 6a represents the dominant direction of propagation for each wave frequency. For the above mentioned spectral peaks, the wave directions are 105° and 95° from the north.

Table 1 lists the wave-field characteristics as derived from SAR images and from *in situ* measurements. The differences in wavelength were 5.7% (8m difference) in the primary wave system and 3.5% (4m difference) in the secondary wave system. The differences of wave direction were 20° and 8°, respectively. In Figs. 5a and 6a, clearly indicates that their spectra shapes are compatible, despite the small difference in the relative magnitude of the spectral peaks. At 25% level of the spectral maximum, the wave energy in the SAR spectrum ranges between 0.06 and 0.16 Hz. Moreover, the wave energy in the wave-rider spectrum ranges between 0.08 and 0.12, with the significant wave height and the wave period being 1.65 m and 8.4 sec, respectively.

4.2. Case(b) : wave field on November 15, 1993

Figure 4b shows another example of applying 2D wavenumber power spectrum SAR image. A primary wave system on November 15, 1993 is represented by the spectral peak at $(n_x, n_y)=(2, 7)$. Table 1 lists wave directions, wavelengths, and wave periods. Two spectral peaks in the omnidirectional frequency spectrum (Fig. 5b) are (1) fp=0.113 Hz corresponds to the wave system $(n_x, n_y)=(2, 7)$ in 2D wavenumber power spectrum, and (2) fp=0.147 Hz does not appear clearly in the wavenumber spectrum. If we limit the search along a circle with a wavelength of 70 m in Fig.

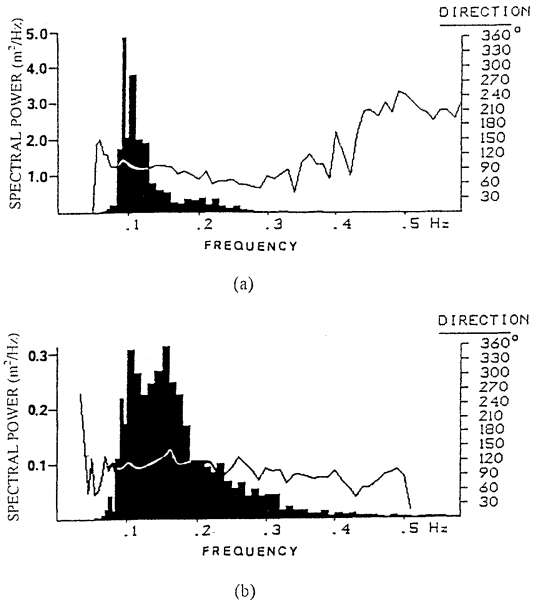

Fig. 6. Frequency power spectra of Hwalien coastal zone derived from *in situ* wave data for case (a) and (b). Solid lines denote wave directions varying with wave frequencies.

4b, then the secondary wave system is found at $(n_x, n_y) = (8, 8)$. The k_x axis is 12.9° in the counter-clockwise direction from the south for a SAR image of ascending pass of ERS-1. Therefore, this wave system came from a 45° counter-clockwise direction from k_x axis, i.e., 122° clockwise direction from the north.

Two spectral peaks were found in the frequency power spectrum (Fig. 6b) of *in situ* wave data. Case (b) of Table 1 lists the wave characteristics analyzed from SAR image and *in situ* wave data. The differences in wavelength and wave direction are 7.6% (or 9m) and 26° for the primary wave system, respectively, and 16% (or 10 m) and 20° for the secondary wave systems. A comparison of both frequency power spectra in Figs. 5b and 6b reveals that their spectral peaks correspond well to each other. The primary wave energy was concentrated within the frequency of 0.09~0.17 Hz in SAR power spectrum and 0.09~0.19 Hz in the power spectrum of *in situ* data. Both spctrum curves were strikingly similar. The sea state was relatively calm with the significant wave height measured by the wave-rider being 0.73 m at a period of 6.6 sec.

5. Conclusions

Microwave remote sensing of the earth's surface has nearly all-weather imaging capabilities, and is insensitive to natural illumination (day or night) or atmospheric conditions (clear or cloudy sky, calm or windy weather). Satellite SAR can image the surface wave-field in severe sea states and obtain information regarding wave characteristics over a vast region. This study has verified the feasibility of using SAR to observe the ocean wave-field over intermediate water depth with a significant wave height below 2 meters. Experimental results demonstrate that an appropriate size of SAR image should be carefully determined for spectral analysis. A subscene of 800 m by 800 m was selected such that the power spectra

Table 1. Comparison of Hwalien wave characteristics derived from ERS-1 SAR and *in situ* wave data for case (a) of November 26, 1993, and case (b) of November 15, 1993.

Sensors	dominant wave systems	wavelength (m)	wave direction (degree)	frequency (Hz)	period (sec)
case (a)					
ERS-1/SAR	primary	149	125°	0.092	10.9
	secondary	110	87°	0.113	8.9
Wave-rider	primary	141	105°	0.095	10.5
	secondary	114	95°	0.110	9.1
case (b)					
ERS-1/SAR	primary	110	93°	0.113	8.9
	secondary	71	122°	0.147	6.8
Wave-rider	primary	119	119°	0.107	9.4
	secondary	61	142°	0.160	6.3

shows stable features. Dispersion relation of deep water waves can be applied in the open sea ; however, the full wave dispersion relation should be used for the coastal zone. High pass and low pass filters were necessary in the preprocessing of SAR images to remove the trend and noises and to improve the SNR of the spectra peaks.

A comparison of main waves derived from SAR images and from *in situ* observation revealed that the difference in wavelength is about 3.5% to 16% (i.e. 4m to 10m) for wavelength of 60 m~150 m, and the difference in wave direction is about 8° to 26°. This finding demonstrates that ERS-1 SAR images are sufficient to examine wave characteristics such as the wavelengths and directions. In these case studies, SAR spectra and *in situ* wave spectra correlated well with each other. Also, the wave energy distribution (spectral shape) and the spectral peaks in the frequency domain were very similar.

Because the power spectra was derived from the SAR images of radar backscattering cross section of the sea surface, the wave height information is combined with other forcings such as the surface wind velocity. Therefore, the wave height could not be estimated directly from the SAR images unless a calibrated MTF is available for corresponding the surface waves and SAR frequency power spectra. Determining the wave height by SAR data is to be addressed in our near future study.

Acknowledgments

The authors would like to thank the Remote Sensing Technology Planning and Developmental Committee, Council of Agriculture, Republic of China, and the National Science Council for financial support of this manuscript under contract Nos. 83-RS-01-22, 84-RS-02-04, 85-RS-02-03 and NSC84-NSPO (A) -OCI-001-01. CSRSR and IHMT made this research possible by providing ERS-1 SAR images and *in situ* wave data. Dr Kai-Yi Huang is also appreciated for his valuable discussion.

References

ALPERS, W. and C. BRÜNING (1986): On the relative importance of motion-related contributions to the SAR imaging mechanism of ocean surface waves, IEEE Transactions on Geoscience and Remote Sensing, Ge-24, 873–885.

ALPERS, W. and K. HASSELMANN (1978): The two-frequency microwave technique for measuring ocean-wave spectra from an airplane or satellite, Boundarylayer Meteorology, **13**, 215–230.

ALPERS, W., D. B. ROSS. and C. L. RUFENACH (1981): On the detectability of ocean surface waves by real and synthetic aperture radar, Journal of Geophysical Research, **86**, C7, 6481–6498.

GONZALES, F. I., R. C. BEAL, W. E. BROWN, P. S. DELEONIBUS., J. W. SHERMAN Ⅲ, J. F. R. GOWER, D. LICHY, D. B. ROSS, C. L. RUFENACH and R. A. SHUCHMAN (1979): Seasat Synthetic Aperture Radar: Ocean wave detection capabilities, Science, **204**, 1418–1421.

HASSELMANN, K., R. K. RANEY, W. J. PLANT, W. ALPERS, R. A. SHUCHMAN, D. R. LYZENGA, C. L. RUFENACH and M. J. TUCKER (1985): Theory of Synthetic Aperture Radar ocean imaging: A MARSEN view, Journal of Geophysical Research, **90**, 4659–4685.

JAIN, A., G. MEDLIN and C. WU (1982): Ocean wave height measurement with SEASAT SAR using speckle diversity, IEEE Journal of Oceanic Engineering, OE-7, No. 2, 103–108.

POPULUS, J., C. ARISTAGHES, L. JONSSON, J. M. AUGUSTIN and E. POULIQUEN (1991): The use of SPOT data for wave analysis. Remote Sensing of Environment, **36**, 55–65.

TUCKER, M. J. (1991): The relation between frequency and wavenumber spectra. Waves in Ocean Engineering: measurement, analysis, interpretation, 431pp, Ellis Horwood, England.

Received June 25, 1995
Accepted February 10, 1996